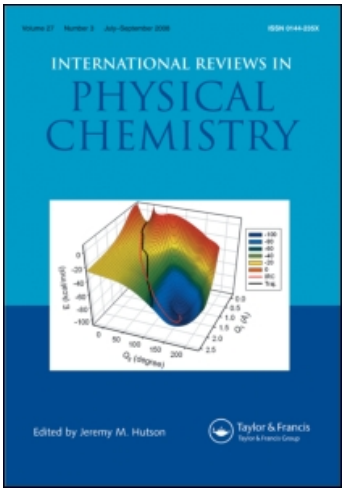

International Reviews in Physical Chemistry
Publication details, including instructions for authors and subscription information:
http://www.informaworld.com/smpp/title~content=t713724383

Study of organized and biological systems using an ultrafast laser

Subhadip Ghosh[a]; Ujjwal Mandal[a]; Aniruddha Adhikari[a]; Shantanu Dey[a]; Kankan Bhattacharyya[a]
[a] Department of Physical Chemistry, Indian Association for the Cultivation of Science, Jadavpur, Kolkata 700 032, India

To cite this Article Ghosh, Subhadip , Mandal, Ujjwal , Adhikari, Aniruddha , Dey, Shantanu and Bhattacharyya, Kankan(2007) 'Study of organized and biological systems using an ultrafast laser', International Reviews in Physical Chemistry, 26: 3, 421 — 448
To link to this Article: DOI: 10.1080/01442350701416888
URL: http://dx.doi.org/10.1080/01442350701416888

International Reviews in Physical Chemistry,
Vol. 26, No. 3, July–September 2007, 421–448

Taylor & Francis
Taylor & Francis Group

Study of organized and biological systems using an ultrafast laser

SUBHADIP GHOSH, UJJWAL MANDAL, ANIRUDDHA ADHIKARI, SHANTANU DEY and KANKAN BHATTACHARYYA*

Department of Physical Chemistry, Indian Association for the Cultivation of Science, Jadavpur, Kolkata 700 032, India

(*Received 2 March 2007; in final form 24 April 2007*)

In an aqueous solution, weak ('soft') molecular interactions lead to the formation of many supramolecular assemblies. In such an assembly, the reactive chemical species remain confined in a nanocavity. Confinement and the local interactions render chemistry in these assemblies markedly different from that in an ordinary solution. Very recently, ultrafast time resolved spectroscopy has been applied to unravel the dynamics in these systems. The new experiments and the computer simulations reveal many surprising and highly interesting features. First, in such a confined system there is almost invariably a new ultraslow component which is slower by 100–1000 times compared to bulk water. Second, in spite of the restrictions imposed inside a nanocavity, dynamics of several processes displays an ultrafast component (in < 10 ps time scale). In this review, we discuss five ultrafast processes in many organized and biological systems. The ultrafast processes include solvation dynamics, proton transfer, energy transfer (FRET), electron transfer and anisotropy decay.

Contents

*Corresponding author. Email: pckb@mahendra.iacs.res.in

International Reviews in Physical Chemistry
ISSN 0144–235X print/ISSN 1366–591X online
http://www.tandf.co.uk/journals
DOI: 10.1080/01442350701416888

1. Introduction

Weak molecular interactions play a key role in many natural processes. The delicate balance between hydrophobic and hydrophilic interactions results in the formation of many nanostructures and self-assembly. Examples of these include the unique native form of a protein, DNA double helix, and numerous supramolecular assemblies (such as micelles or guest–host complexes). The importance of these nanostructures is fairly diverse and range from molecular recognition (e.g. enzyme–substrate, antigen–antibody interaction) to a more general issue of unusual chemistry in confined environments. In a self-organized or biological assembly, the reactive chemical species is confined in a small cavity of dimension a few nanometres (nm) (e.g. in the hydrophobic pocket of an enzyme). Confinement in such a nanocavity affects chemistry in several ways. First, confinement results in close proximity of the reactants which can markedly accelerate bi-molecular reactions. Second, in such a nanocavity the reactant is often bound to the macromolecular host by hydrogen bonds or weak van der Waals interaction. Third, many properties of the solvent molecules (in most cases water) are dramatically modified in a confined system.

Most recently, many groups have applied ultrafast laser spectroscopy to unravel dynamics in self-organized and biological systems [1–6]. These studies reveal many interesting and hitherto unknown features of ultrafast chemical processes in a confined system. In this review, we will summarize the most recent results on this rapidly growing subject. The plan of the review is as follows. In section 2, we give a brief overview of the structures of some organized assemblies. This discussion is essential to understand how confinement and local interactions affect ultrafast dynamics. In the subsequent sections, we will discuss five ultrafast processes in many confined systems. These processes include solvation dynamics, excited state proton transfer, photoinduced electron transfer, fluorescence resonance energy transfer (FRET), and fluorescence anisotropy decay. A host of different experimental and theoretical strategies have been employed to study dynamics in self-organized assemblies. In this article, we will mainly

focus on application of ultrafast time-resolved fluorescence spectroscopy with occasional references to other experimental techniques, theory and computer simulations. For a general discussion on fundamentals of fluorescence spectroscopy we refer to an excellent text book [7].

2. Structure of organized assemblies

The biological function of a system crucially depends on the structure as well as dynamics. Because of this, structural biology received very serious attention for over 70 years (since the mid-1930s). The main technique of structure determination is obviously X-ray diffraction. However, many nanostructures are formed only in solution where X-ray diffraction is inapplicable. Structure of a supramolecular assembly in a liquid is best determined by small angle neutron scattering (SANS) [8] and also by light scattering [9, 10]. Structures of some common self-organized systems are shown in figure 1.

2.1. *Cyclodextrin*

Perhaps the simplest example of a self-organized system is a host–guest complex involving a cyclodextrin as a host (figure 1a). A cyclodextrin is a cyclic polymer containing 6 (α-), 7 (β-) or 8 (γ-) glucose units. A cyclodextrin is a torus shaped nanovessel with a height $\sim$8 Å and a largest diameter of $\sim$4.5 Å (for α-), $\sim$6.5 Å (for β-) and $\sim$8Å (for γ-) [11]. They are moderately soluble in water and more soluble in any other polar solvents (e.g. dimethylformamide, DMF). The interior of a cyclodextrin is hydrophobic and resembles a cyclic ether. As a result, in an aqueous solution a cyclodextrin encapsulates many organic molecules. Because of this property, cyclodextrin has versatile applications in solubilizing insoluble drugs in water and in targeted drug delivery [12]. During drug delivery across a membrane, a membrane surfactant gets insert into the cyclodextrin cage dislodging the drug (guest) molecule. Compared to an unsubstituted cyclodextrin, a *O*-methyl or a *O*-hydroxypropyl derivative of a cyclodextrin is much more soluble and hence, is more useful in drug delivery [12]. The substituted cyclodextrins have also been applied to prevent misfolding of a protein by encaging the hydrophobic aromatic residues [13].

2.2. *Micelles*

A micelle refers to a nearly spherical aggregate of a surfactant. Such an aggregate is formed in an aqueous solution (or in a few highly polar solvents) above a threshold surfactant concentration known as critical micellar concentration (CMC). According to SANS [8] and light scattering [9, 10] studies a micelle consists of a hydrophobic core consisting of the alkyl chains and a hydrophilic corona containing the polar head groups, counter ions and large number of water molecules. Tri-block co-polymer micelles have received considerable recent attention because of their interesting

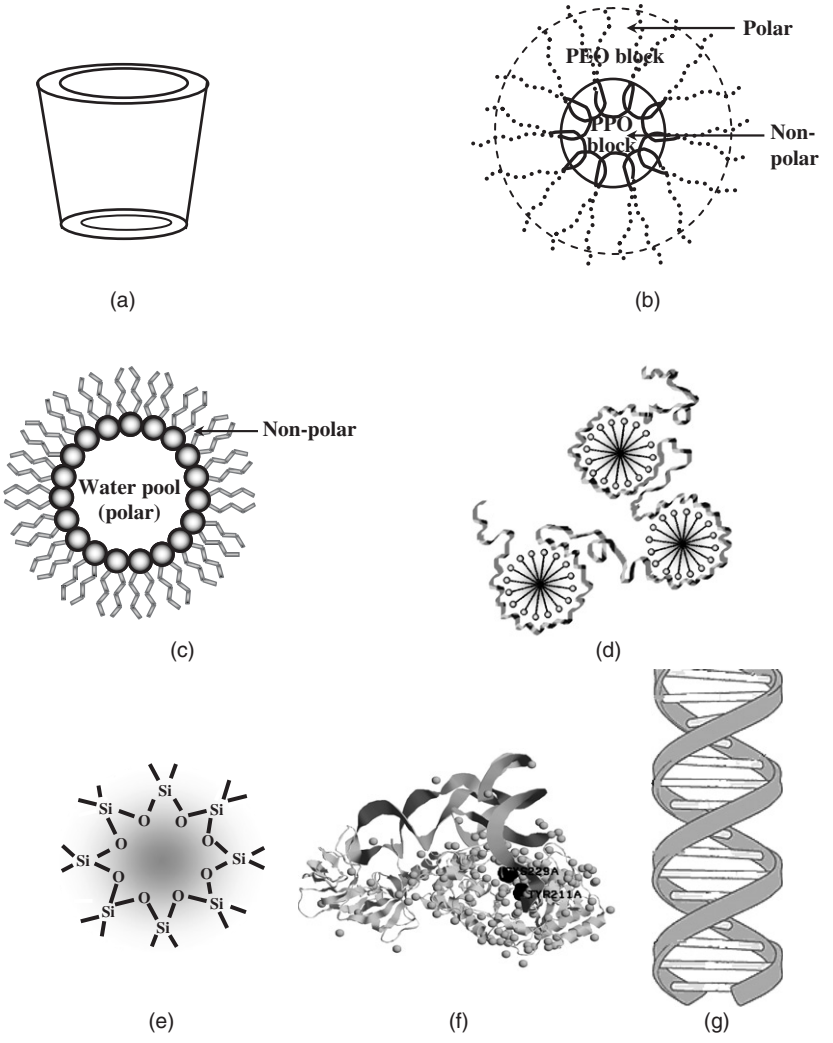

Figure 1. Structure of some organized assemblies: (a) cyclodextrin, (b) tri-block co-polymer micelle, (c) reverse micelle, (d) polymer–surfactant aggregate, (e) sol–gel glass, (f) protein, and (g) DNA.

self-assembly and diverse phase behaviour [14–17]. A tri-block co-polymer micelle consists of a hydrophobic polymer segment (e.g. polypropylene oxide, PPO) as core and a hydrophilic block (e.g. polyethylene oxide, PEO) as corona. The co-polymer $(PEO)_{20}$–$(PPO)_{70}$–$(PEO)_{20}$ is known as Pluoronic P123. According to SANS studies, a P123 micelle consists of a hydrophobic core of PPO block with a diameter of 96 Å and a hydrophilic corona of thickness 46 Å containing the PEO block (figure 1b) [14, 15]. The marked variation of polarity over a short distance in different regions (PPO and PEO blocks) of a P123 micelle has many interesting implications. For instance, absorption maximum of a polarity sensitive probe is different in different regions of P123 micelle. Thus by varying the excitation wavelength one may excite probes in different regions of

the micelle. We will discuss later in this review, how solvation dynamics and FRET in different regions of a P123 micelle may be studied using this principle.

2.3. *Reverse micelle*

A reverse micelle is a micellar aggregate where the bulk medium is a non-polar solvent (alkane) (figure 1c) [18–20]. In such an aggregate the polar head groups of the surfactants point inward and the non-polar alkyl chains point outward. In a reverse micelle, a polar solvent (e.g. water, acetonitrile or DMF) may be encapsulated inside the aggregate in form of a 'water (solvent) pool.' For an AOT (aerosol-OT, dioctylsulfosuccinate, sodium salt) microemulsion, the radius of the nanodroplet (water pool) is roughly equal to $1.5w_0$ (in Å) where w_0 is the number ratio of the water and the surfactant (AOT) molecules [18]. In a microemulsion, the non-polar bulk hydrocarbon is separated from the highly polar water pool by a layer of surfactants. Thus the property of the microenvironment changes rapidly over a distance roughly equal to length of the surfactant (AOT) molecule. The water pool in a microemulsion is a fascinating model of confined water. Recently, the water pool has been subject of many experiments and computer simulations. Levinger and co-workers [20] studied the water pool of AOT reverse micelles with a highly charged decavanadate (V-10) oligomer using V-51 NMR spectroscopy. From V-51 chemical shifts, they inferred that the V-10 is deprotonated even when an acidic solution of protonated V-10 is encapsulated in a reverse micelle. This is consistent with a decreased proton concentration in the intramicellar water pool and presence of a proton gradient inside the reverse micelles. In this case the interfacial region (near the AOT anion) is acidic with high proton concentration while the core of the water pool (where vanadate exists) is neutral [20]. Fayer and co-workers studied the water pool using ultrafast infrared spectrally resolved pump–probe and vibrational echo spectroscopies [21]. They showed that a weighted sum of the core and shell components reproduces the size dependent spectra and the non-exponential population relaxation dynamics [21]. Owrutsky and co-workers studied confinement effects on anion vibrational spectra and dynamics in the water pool using ultrafast infrared spectroscopy [22].

2.4. *Polymer–surfactant aggregate*

Interaction of a surfactant with a polymer (e.g. a protein) has important implications in surfactant induced unfolding of a protein or interaction of a protein with a bio-membrane. When a polymer interacts with a surfactant often large aggregates are formed at a surfactant concentration far below the CMC of the surfactant. The minimum surfactant concentration needed for the formation of such an aggregate is called critical association concentration (CAC). The size of a polymer–surfactant aggregate is found to be larger than that of the polymer or of the micelle [23]. It has been suggested that a polymer–surfactant aggregate has a 'necklace' like structure with small micelles as 'beads' which are connected by the polymer chain as 'threads' (figure 1d). The properties of such an aggregate are quite different from those of a micelle because the polymer chain shields the micelle from bulk water and also reduces repulsion between the polar head groups.

2.5. *Sol–gel glass*

A sol–gel glass is formed at ambient temperature (i.e. by a soft route) through hydrolysis and subsequent condensation of tetra-alkyl orthosilicates [24]. Alcohol is produced as a by-product of hydrolysis. A sol–gel glass (figure 1e) consists of nanopores whose size may be varied depending on condition (pH) of the hydrolysis. Water along with other organic molecules may be trapped in the nanopores of a sol–gel glass. Many organic assemblies (e.g. protein, micelle or lipid) may also be encapsulated inside a sol–gel glass [24–26]. Such organic doped glass is known as ormosil and has versatile applications in photonics. Fourkas and co-workers along with several other groups studied dynamics of several liquids in the nanopores of sol–gel glass using optical Kerr effect [3]. They observed a slow component which they attributed to binding of the liquids to the surface of the sol–gel glass.

3. Solvation dynamics

Solvation dynamics describes the dynamic dielectric response of a polar solvent towards creation of a dipole (or more properly, large change in the dipole moment of a solute). A dipole may be suddenly created in a solution by excitation of a suitable solute (probe) using an ultrashort laser pulse. For this experiment, a suitable solute is one whose dipole moment is very small in the ground state but is very large in the excited state. The dynamic response of the solvent molecules is not instantaneous. The solvent molecules gradually rearrange and reorient around the dipole in the excited state (figure 2). As a result, the energy of the excited solute dipole decreases with increase in time and the fluorescence maximum of the solute displays a time dependent red shift. This is known as dynamic Stokes shift (DSS). The fluorescence decays of a solute, undergoing

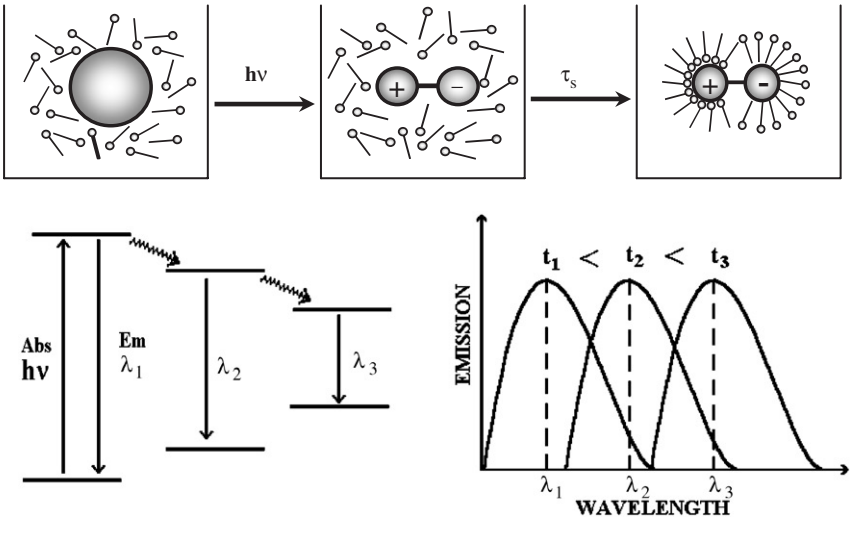

Figure 2. Solvation and time dependent fluorescence Stokes shift.

solvation dynamics, exhibit a marked dependence on the wavelength. Emission at a short wavelength arises from the unsolvated species and hence, at short wavelength a decay is observed. The solvated species emit at a long wavelength and a rise precedes the decay. The rise at a long wavelength represents a clear signature of solvation dynamics. Solvation dynamics is monitored by the decay of the solvent response function, $C(t)$ which is defined as,

$$C(t) = \frac{\nu(t) - \nu(\infty)}{\nu(0) - \nu(\infty)} \tag{1}$$

where, $\nu(0)$, $\nu(t)$ and $\nu(\infty)$ are the observed emission frequencies at time zero, t and infinity, respectively.

In bulk water, solvation dynamics is extremely fast with a major component in 0.1 ps (100 fs) time scale and a minor component of 1 ps [27–29]. According to continuum theory, the solvation time (τ_s) is given by [4]

$$\tau_s^{-1} = 2D_R\left[1 + \left(\frac{D_T k^2}{2D_R}\right)\right]. \tag{2}$$

For water, the translational diffusion coefficient, $D_T = 2.5 \times 10^{-9}\,m^2\,s^{-1}$, rotational diffusion coefficient, $D_R = 2.2 \times 10^{11}\,s^{-1}$ and $k \sim 2\pi/1.5\sigma$, with diameter of water molecule, $\sigma \sim 2.8$ Å. Using these parameters, $\tau_s \sim 1$ ps in bulk water. The continuum picture however, does not describe the major sub-100 fs component of solvation dynamics. This component has been ascribed to intermolecular vibration and libration of the extended hydrogen-bond network in bulk water [28].

Interestingly, solvation dynamics of water confined in many organized and biological assemblies displays a component in 100–1000 ps time scale [1–6]. The ultraslow component of solvation dynamics suggests that nanoconfined water ('biological water') is substantially slower and fundamentally different from ordinary water. In the following sections, we will discuss some recent results in many organized and biological systems. Experimentally, the ultraslow component of relaxation of biological systems was first indicated in the early dielectric relaxation studies [4]. There is an ongoing debate on whether the slow dynamics is due to dynamics of the macromolecular chains with associated polar groups and water molecules or whether it is due to the water alone. Before discussing the actual results we will briefly outline a few theoretical models and more recent computer simulations which give a better perspective on the physical origin of the ultraslow dynamics.

3.1. *Origin of ultraslow dynamics of biological water*

The first hydration shell of a protein contains a large number of water molecules which are hydrogen bonded to the protein. Water molecules 'bound' to a large biological macromolecule are largely immobilized. In contrast, the 'free' water molecules which are not hydrogen bonded the macromolecule retain bulk water like high mobility (figure 3). On the basis of NOE studies, Wuthrich and co-workers first

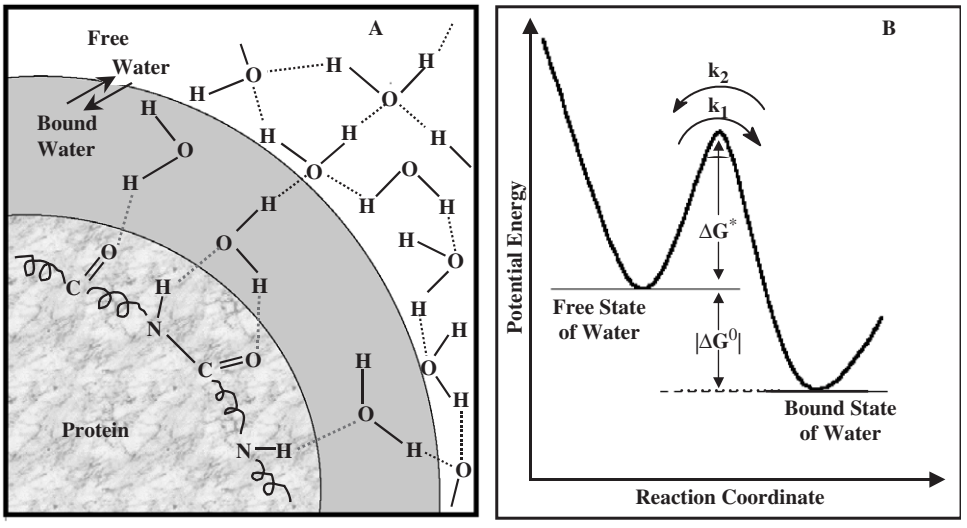

Figure 3. (a) Free and bound water in the hydration shell of a protein. (b) Potential energy diagram for dynamic equilibrium between free and bound water. (Reprinted with permission from [4]. Copyright © 2003 American Chemical Society.)

qualitatively proposed that the water molecules near a protein may be classified as 'bound' and 'free' water [30]. Nandi and Bagchi developed a phenomenological theory which suggests that the ultraslow dielectric response of a protein arises because of a dynamic exchange between the bound and free water [31]. According to this model, the rate determining step in solvation dynamics is the rate of interconversion of bound-to-free water (k_2),

$$k_2 = \left(\frac{k_B T}{h}\right) \exp\left(\frac{-(\Delta G^0 + \Delta G^*)}{RT}\right) \tag{3}$$

where, ΔG^* is the activation energy for the conversion of free-to-bound water molecules.

More recently, many groups have applied large scale computer simulations to elucidate the structure and dynamics of the water molecules and the polar residues of a biological system. An early simulation by Levitt and Sharon [32], revealed that there is a clustering of water molecules near a protein which results in an increase of density by 25% (i.e. up to 1.25). A more recent computer simulation by Bagchi and co-workers suggests that a water molecule 'bound' to a micelle is stabilized by about 8 kcal/mol compared to bulk (free) water [33]. Most recently, Golosov and Karplus examined the contribution of the solvent (bulk water and ion), bound water and polar residues of protein [34]. According to their simulation, the long (~100 ps) component of polar solvation dynamics arises from coupled hydration and protein conformational dynamics. We will discuss these results in more detail in a following section along with the experimental results.

Benjamin and co-workers carried out a detailed simulation of dynamics of water molecules at a liquid–liquid interface [35, 36]. These simulations suggest that the solvation dynamics at a liquid–liquid interface exhibits a slow component which is absent in bulk water or at the water–vapor interface and also depends on the distance from the interface [36].

The slow dynamics may also originate from Rouse chain dynamics of a homopolymer along with polar residues and associated water molecules. According to this model, the time correlation function for the chain's solvation energy fluctuations is a multi-exponential function $\Sigma a_i \exp(-t/\tau_i)$ where τ_i $(= \lambda_i^1)$ are given by [37]

$$\lambda_i = 3D_0\left(\frac{l\pi}{Nb}\right)^2 \tag{4}$$

where N is the number of monomers in the chain and $l = 1, 3, 5, \ldots, N-1$, b^2 is the mean square bond length, D_0 is the translational diffusion coefficient of a monomer.

Another source of slow decay could be self-diffusion of the solvation probe. A solute (non-polar in the ground state) is supposed to be localized in the relatively non-polar region of an organized assembly. On excitation when the dipole moment of the solute increases the probe may migrate to a more polar region of the assembly. In the following sections we will try to distinguish different cases where the different mechanisms of slow dynamics apply.

3.2. *Solvation dynamics in the nanocavity of a cyclodextrin*

Dynamics of a few (~10) water molecules in the nanocavity of a cyclodextrin is interesting in many respects. First, this situation roughly corresponds to a solute with an incompletely formed first solvation shell. Second, the translation and rotation of water may be completely frozen [38]. Fleming and co-workers reported that solvation dynamics of water inside an unsubstituted γ-cyclodextrin cavity exhibits three components of 13 ps, 109 ps and 1200 ps [39]. They ascribed the slow components of solvation dynamics to three processes. First, the restricted motion of the highly confined water molecules, second, the motion of the guest probe molecule in and out of the cavity, and third, the fluctuations of the γ-cyclodextrin ring. They also observed a substantial amount of dynamic Stokes shift. This is consistent with the general view that solvation dynamics gives local dielectric response with >90% of solvation being accounted for the first solvation layer.

More recently, Sen *et al*. studied the effect of methyl substitution of cyclodextrin on ultrafast solvation dynamics [40]. In tri-methyl β-CD, all the three OH groups of the β-CD cavity are replaced by OMe groups. It is observed that compared to unsubstituted β-CD solvation dynamics in tri-methyl β-CD is significantly slower and displays two very slow components – 240 ps (45%) and 2450 ps (31%) – along with a fast component of 10 ps (24%). In contrast, dimethyl β-CD (which contains one OH group per glucose unit) exhibits much faster dynamics with a major (40%) ultrafast component (<0.3 ps), a fast component of 2.4 ps (24%) and two slow components – 50 ps (18%) and 1450 ps (18%).

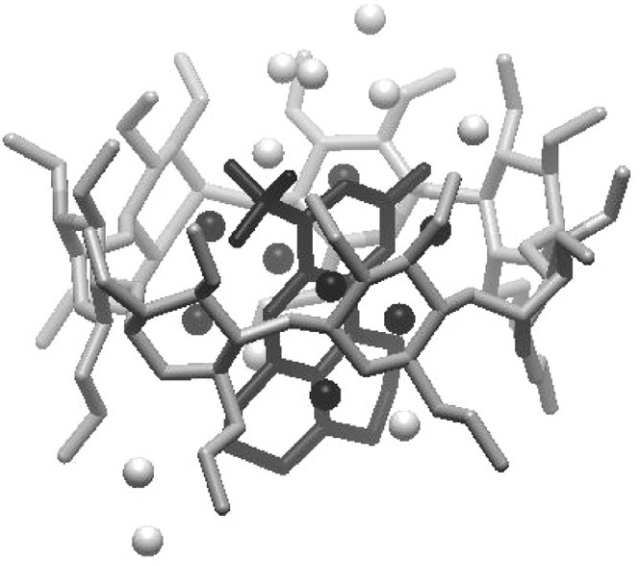

Figure 4. Structure of a supramolecule containing tri-methyl-β-cyclodextrin, C153, and water molecules (optimized by MM2). Black spheres represent the water molecules inside the cavity and white spheres, represent those outside the cavity.

Figure 4 shows the structure (optimized using MM2) of a supramolecule consisting of tri-methyl-β-cyclodextrin with C153 along with water molecules inside and outside the cavity. In this case, the minimum O–O distance between a water molecule inside the cavity to another outside is $\sim$7.7 Å. The large (7.7 Å) distance suggests that there is no hydrogen-bond network connecting water molecules inside the cavity to those outside. For water molecules inside the cavity the O–O distance is $\sim$2.4 Å which suggests strong hydrogen bonding.

Ultrafast solvation dynamics in bulk water arises from the extended hydrogen bonded network [28]. In the case of unsubstituted CDs, a similar network is established between the water molecules inside the cavity with those outside the cavity through the OH group of the cyclodextrins. Hence, a major portion of solvation dynamics displayed in an unsubstituted cyclodextrin is ultrafast ($<$2 ps). In the case of tri-methyl β-CD, there are no OH groups at the rim of the cyclodextrin cavity. Thus there is no hydrogen-bond network connecting the water molecules inside the cyclodextrin cavity and those outside the cavity. As a result, the ultrafast component ($\leq$2 ps) vanishes almost completely in tri-methyl β-CD. In this case, the fastest component is 10 ps with 24% contribution [40]. Because of the presence of seven OH groups at the rim of dimethyl β-CD, the hydrogen bond network is at least partially established. Thus in this case, there is a major (64%) ultrafast component ($\leq$0.3 and 2.4 ps) of solvation dynamics [40].

Sen *et al.* studied solvation dynamics of a non-aqueous solvent, dimethylformamide (DMF) in a β-cyclodextrin cavity [41]. The dynamics of confined DMF molecules is found to be described by two slow components of 400 ps and 8000 ps. This is substantially slower than the solvation ($\sim$1 ps) in bulk DMF and displays an ultraslow component of $\sim$8000 ps [41].

3.3. *Solvation dynamics in micelles and vesicles: excitation wavelength dependence*

In this section we will review the result on solvation dynamics in micelles, reverse micelles and lipid vesicles. About a decade ago, it was discovered that solvation dynamics in these surfactant assemblies exhibits a component in 100–1000 ps time scale which is slower by 2–3 orders compared to bulk water [3, 4]. Note, in micelles there is always a bulk like ultrafast component. The relative contribution of the ultraslow and ultrafast component in a micelle varies from system to system.

In order to verify the dynamic exchange model (equation 3) in the case of a micelle, Sen *et al*. studied temperature dependence of solvation dynamics in a micelle, triton X-100 (TX-100) [42]. They found that with rise in temperature solvation time in TX-100 micelle decreases from 800 ps at 283 K to 100 ps at 323 K. They also observed that the plot of logarithm of average solvation time against $1/T$ is linear. From this plot the activation energy of solvation dynamics is found to be 9 ± 1 kcal mol^{-1} with a positive entropy factor of 14 cal k^{-1} mol^{-1} [42]. It is interesting to note that the activation energy obtained experimentally from temperature dependence of solvation dynamics is very close to the difference between water–water and micelle–water hydrogen bond energy, estimated in a computer simulation [33]. Similar linear plots are observed for a cyclodextrin aggregate [43] and in a protein [44].

Most recently, there have been several attempts to study solvation dynamics in different regions of a micelle (i.e. to spatially resolve dynamics) using excitation wavelength dependence. An organized assembly is highly heterogeneous with polarity and other properties varying over molecular length scale. Evidently, the absorption and emission maxima of a polarity sensitive probe are different in different regions of such an assembly. The probe molecules in different locations of an organized assembly may be selectively excited by varying the excitation wavelength (λ_{ex}). At a relatively short excitation wavelength ('blue edge') the probe molecules residing in a non-polar region are preferentially excited and this gives rise to a blue shifted emission spectrum. Excitation at a longer wavelength ('red edge') selects the probe in a polar region of the assembly and results in a red shifted emission spectrum. Such a shift of the emission maximum with variation of excitation wavelength (λ_{ex}) is known as red edge excitation shift (REES) [45–47].

Until recently REES is mostly used to study variation of steady state spectra. Very recently, REES has been utilized to study dynamics in different regions of reverse micelle, lipid vesicles, micelle and a gel. Satoh *et al*. investigated λ_{ex} dependence of solvation dynamics of coumarin 343 (C343) in the water pool of an AOT reverse micelle [48]. They observed that the dynamic Stokes shift ($\Delta\nu$) decreases with increase in the excitation wavelength. To explain this, it is proposed that the probe molecules are distributed broadly over two environments. The first environment is a bulk-water like region in the core of water pool where solvation dynamics occurs on a sub-100 ps time scale. The other is a region in the vicinity of the surfactant head-group where the dynamics is much slower (700 and 2000 ps). Excitation at the red end of the absorption spectrum preferentially selects the probes in the bulk-like region. The sub-100 picosecond dynamics in this region remains undetected in a picosecond set up and hence, $\Delta\nu$ decreases with increase in λ_{ex}.

In a lipid vesicle, a highly hydrophobic bilayer membrane of surfactants encloses a polar water pool. Sen *et al*. studied λ_{ex} dependence of solvation dynamics of coumarin

480 (C480) in a DMPC vesicles using a picosecond [49] and a femtosecond [50] set up. For $\lambda_{ex} = 390$–430 nm, solvation dynamics in a lipid displays an ultrafast component (<0.3 ps) and a fast component (1.5 ps) along with two slow components – 250 ps and 2000 ps. With increase in λ_{ex}, the relative contribution of the ultrafast components (<0.3 ps and 1.5 ps) increases from 48% at $\lambda_{ex} = 390$ nm to 100% at $\lambda_{ex} = 430$ nm. Thus, at $\lambda_{ex} = 430$ nm, there is no slow component. The ultrafast dynamics is ascribed to the very polar and mobile bulk-like region, deep inside the water pool. The slow dynamics (250 ps and 2000 ps) arises from a restricted interfacial region inside the bi-layer membrane.

A tri-block co-polymer micelle (e.g. PEO_{20}–PPO_{70}–PEO_{20}, pluoronic P123) consists of a slow, hydrophobic and non-polar PPO core and a polar, fast bulk-like peripheral corona containing the PEO block (figure 1b). Sen *et al.* studied solvation dynamics in different regions of a P123 micelle by varying λ_{ex} [51]. With increase in λ_{ex} from 345 nm to 435 nm, the emission maximum of C480 exhibits a large red edge excitation shift (REES) by 25 nm. With increase in λ_{ex}, solvation dynamics in P123 micelle becomes faster. The λ_{ex} dependence in P123 micelle has been interpreted in terms of three regions – the fast PEO–water interface with solvation time ≤ 2 ps, chain region (60 ps) and a very slow (4500 ps) hydrophobic core region (PPO–PEO interface). With increase in λ_{ex}, contribution of the bulk-like ultrafast dynamics (≤ 2 ps) increases from 7% at $\lambda_{ex} = 375$ nm to 78% at $\lambda_{ex} = 425$ nm with a concomitant decrease in the contribution of the core-like slow component (4500 ps) from 79% at $\lambda_{ex} = 375$ nm to 17% at 425 nm. Contribution of the 60 ps component, which arises from chain dynamics, decreases from 14% at $\lambda_{ex} = 375$ nm to 5% at $\lambda_{ex} = 425$ nm [51].

Most recently, Ghosh *et al.* studied the λ_{ex} dependence of solvation dynamics in the 'solid' cubic gel phase of P123 [52]. It is observed that even in the 'solid' phase there is a bulk water like ultrafast component (≤ 2 ps). The ultrafast component is attributed to the water molecules in voids or pores of the gel. The PPO core in a gel gives rise to very long component of 4500 ps (figure 5). There is a third component of 500 ps which is ascribed to chain–chain entanglement. With rise in λ_{ex} contribution of the bulk-like ultrafast component increases and that of the ultraslow component arising from the core decreases (figure 5).

Usually, micelles are formed in a polar solvent (e.g. water, methanol, acetonitrile etc). Most recently, many groups reported formation of micelles [53] and reverse micelles [54] in ionic liquids (IL). Petrich and co-workers studied solvation dynamics of coumarin 153 in amphiphilic ionic liquids (1-cetyl-3-vinylimidazolium bromide and 1-cetyl-3-vinylimidazolium bis-[(trifluoromethyl) sulfonyl] imide) and their corresponding micelles in water [53]. The magnitude of retardation of solvation dynamics on confinement in a micelle is much smaller in the case of an IL than that in water. Solvation dynamics in ionic liquid is slow and exhibits a nanosecond component. There is a further 2–3 fold increase of solvation time in the micelle in IL [53]. It is proposed that the imidazolium moiety is responsible for the major part of the solvation.

Sarkar and co-workers studied solvent relaxation in [bmim][PF_6]/TX–100/water microemulsion using a hydrophobic probe, coumarin 153 (C153), and a hydrophilic probe, coumarin 151 (C151) [54]. For C153, with an increase in the [bmim][PF_6]/TX-100 ratio (R), the solvent relaxation time does not change much. For C151, with an increase

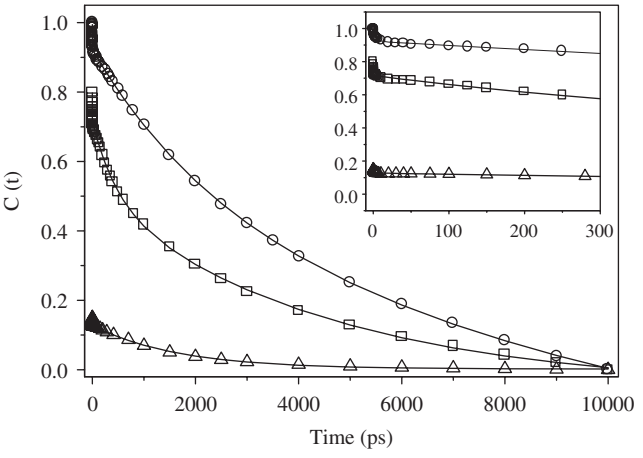

Figure 5. Complete decay of solvent response function $C(t)$ of C480 in P123 gel for $\lambda_{ex} = 375$ nm (○), $\lambda_{ex} = 405$ nm (□) and $\lambda_{ex} = 435$ nm (Δ). The points denote the actual values of $C(t)$ and the solid line denotes the best fit. Initial portions of the decays are shown in the inset. (Reprinted with permission from [52]. Copyright © 2007 American Chemical Society.)

in R the slow component of the solvation time gradually decreases and the fast component gradually increases.

Recently, many groups carried out large scale atomistic computer simulations on micelles [33, 55, 56], reverse micelles [57, 58] and in many nanoconfined systems [59–63]. The dynamics at different regions of the micelle or of different kinds of bound water (singly or doubly hydrogen bonded to the micelle) have been studied in considerable detail in these simulations. One interesting experimental observation is solvation dynamics in a cationic micelle is slower than that in an anionic or a neutral micelle. This is attributed to the binding of the heavier end of water (oxygen) to the cationic head group of a micelle [55]. Another interesting suggestion is that in a reverse micelle following excitation the polar solute with increased dipole moment migrates to another (more polar) region of the reverse micelle. The experimentally observed time dependent decrease in width of the emission spectra has been attributed to such migration (self-diffusion) [64, 65]. Such a motion of the solute in a nanocavity was detected in a computer simulation by Thompson [61] and later in a reverse micelle by Faeder and Ladanyi [57].

3.4. *Solvation dynamics in a protein*

The biological function of a protein is largely controlled by the amino acid sequence, structure and chain dynamics along with the quasi-bound *biological or structured* water molecules near a protein. There are three different strategies to study solvation dynamics in a protein using a fluorescence probe. First, many groups use the amino acid tryptophan as an intrinsic fluorescence probe to study protein dynamics [2]. The photophysics of tryptophan involves interconversion between multiple conformers [66],

internal Stark effect [67] and multiple excited states [68]. This makes tryptophan too complicated a probe for solvation dynamics.

The second approach is to use a non-covalent probe whose location inside a protein may be inferred by measuring its distance from a tryptophan residue using FRET [69–72]. Fleming and co-workers studied solvation dynamics of a non-covalent probe, eosin in the hydration layer of lysozyme using three pulse echo peak shift [69]. They found that while most of the dynamics occurs in sub-picosecond time scale, there is a slow component of 530 ps whose contribution is about 8%. The slow component is absent for free eosin in bulk water and hence, is assigned to protein bound water [69]. The fluorescence dynamic Stokes shift of DCM non-covalently attached to a protein (human serum albumin, HSA) exhibits a slow component (600 ps) and very long component (10 ns, i.e. 10,000 ps) [70]. The 600 ps component is assigned to bound water. The ultraslow 10 ns component may be assigned to overall tumbling of the protein, When the protein (HSA) is incorporated in a lipid vesicle the volume of the system becomes very large and tumbling is too slow to occur within the excited state lifetime of the probe. For HSA in DMPC vesicle the 10 ns component is not detected [71]. This supports the assignment of the 10 ns component to tumbling.

The third approach is to covalently attach a fluorescence probe at selected sites of a protein [73–75]. Guha *et al*. studied solvation dynamics at the active site of an enzyme, glutaminyl-tRNA synthetase (GlnRS) (figure 1f) [75]. For this purpose they attached a fluorescence probe, acrylodan at a cysteine residue C229 near the active site. Solvation dynamics in GlnRs displays two slow components – 400 ps and 2000 ps. When the amino acid glutamine (Gln) binds to the enzyme (GlnRS) the 400 ps component slows down about two-fold to 750 ps while the 2000 ps component remains unchanged. When $tRNA^{gln}$ binds to GlnRS the 400 ps component does not change but the 2000 ps component becomes slower (2500 ps). From this, it is inferred that the 400 ps component arises from the water molecules at the Gln binding site while the 2000 ps corresponds to the $tRNA^{gln}$ binding site. A mutant Y211H-GlnRS was constructed in which the glutamine binding site is disrupted. The mutant Y211H-GlnRS labelled at C229 with acrylodan exhibits significantly different solvent relaxation [75]. This demonstrates that the slow dynamics is indeed associated with the active site.

There is considerable interest to understand the structure and dynamics in the non-native state of a protein. Early NMR studies indicate that there is considerable residual structure present in a partially unfolded states or a molten globule [76]. Sen *et al*. [77] studied solvation dynamics in the molten globule state of a protein using both a covalent and non-covalent probe. In the native state, the covalent probe resides at the surface and exhibits much shorter solvation time (120 ps) compared to that (1400 ps) of a non-covalent probe (bis-ANS) which goes deep inside the protein [77]. However, in the molten globule state when the protein opens up solvation time of both the probe becomes similar (~200 ps) [77].

Dutta *et al*. studied solvation dynamics of coumarin 153 (C153) in lysozyme denatured by a surfactant SDS and dithiothreitol (DTT) [72]. Solvation time of C153 in the native state of lysozyme is 330 ps. Addition of SDS to lysozyme causes destruction of the non-covalent interactions and the protein becomes decorated by small SDS micelles. Under this condition, the average solvation time increases to 7250 ps. This is more than 20 times longer than the average solvation time (330 ps) in the native state

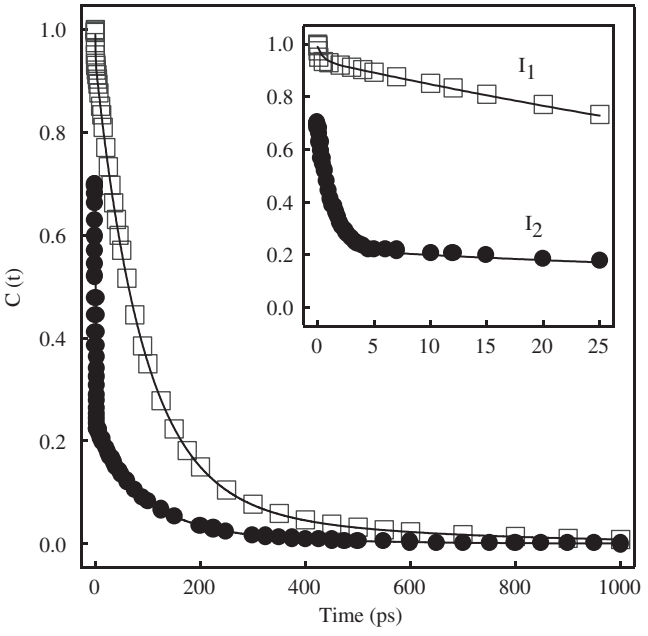

Figure 6. Initial part of the decay of $C(t)$ of C153 containing 5 μM cytochrome C and 2 mM SDS (I_1) (□); 5 μM cytochrome C, 2 mM SDS and 5 M urea (I_2) (●). (Reprinted with permission from [79]. Copyright © 2006 American Chemical Society.)

of lysozyme. When DTT is added to lysozyme denatured by SDS, the di-sulfide bonds are ruptured and the protein assumes an extended polymer like structure so that it easily passes through porous poly-acrylamide gel during gel electrophoresis. For such an extended protein, the average solvation time is 1100 ps [72].

The mitochondrial respiratory membrane protein cytochrome C is cationic in nature and carries a net positive charge (+8) at a neutral pH (~7). Binding of cytochrome C to anionic surfactants (e.g. sodium dodecyl sulfate, SDS) or membranes results in partially folded or molten globule-like states. Cytochrome C forms two partially folded intermediates – I_1 (in the presence of SDS) and I_2 (in the presence of SDS and urea) [78]. Solvation dynamics in these two partially folded states of cytochrome C are found to be drastically different and the most prominent differences are detected at very early times (<20 ps, figure 6) [79]. I_1 displays an ultrafast component – 0.5 ps (5%) and two slow components – 90 ps (85%) and 400 ps (10%). In the case of I_2, there is a major ultrafast component of 1.3 ps (47%) and two slow components – 60 ps (12.5%) and 170 ps (10.5%). The faster solvation dynamics suggests that I_2 is more open and labile compared to I_1 [79]. Samaddar *et al.* studied solvation dynamics in the pre-molten globule state of GlnRS [80]. They observed that the solvation time is of the order, native > molten globule > pre-molten globule.

Sen *et al.* studied solvation dynamics in hen egg white lysozyme in the presence of urea and SDS using coumarin 153 (C153) as a probe [81]. They found that a small amount of SDS (3 mM) causes partial recovery of the urea denatured protein and solvation dynamics in this system is very close to that in the native protein.

However, large excess of SDS (28 mM) causes complete loss of the tertiary structure of the native protein and the SDS micelles are squeezed inside the polypeptide chain of the protein. This results in a 3.5 times retardation of solvation dynamics compared to that in the native state [81].

Very recently, several groups have applied large scale molecular dynamics simulations to elucidate solvation dynamics in different regions of a protein [30, 83–88]. It needs to be emphasized that there are many species which may contribute to the polar solvation dynamics. As noted earlier [32], the large number of water molecules greatly outnumber all the polar residues of a protein. Still one can not ignore the contribution of the polar residues of the protein.

In contrast to the large body of work demonstrating ultraslow dynamics near a protein, incoherent quasi-elastic neutron scattering [89, 90] and NMRD [91] studies suggest very slight retardation of the water molecules near a protein. It should be emphasized that different techniques detect different things. First, dielectric relaxation (DR) and dynamic Stokes shift (DSS) capture collective response of the solvent (water) dipoles. NMRD and QENS describe dynamics of a single water molecule in the absence of an external electric field (e.g. that provided by an instantaneously created solute dipole). Second, NMRD, QENS, and DR offer no spatial resolution and all the water molecules contribute in these experiments. Evidently, the number of quasi-bound water molecules around a fluorescent probe is very small compared to the very large number of water molecules present around a protein. NMRD and QENS data are dominated by the huge number of water molecules, many of which are very fast (particularly those at the surface of a protein). Thus, NMRD and QENS which detect an average of the water molecules at all the sites often report very fast dynamics or almost bulk water like residence times with very small (sometimes negligible) contribution of the slow water molecules. According to a computer simulation by Maroncelli and Fleming [82] the first solvation shell makes a major contribution (85%) to DSS. Thus, DSS is dominated by dynamics of the water molecules in the first solvation shell around the solute and hence, provide high spatial resolution. In summary, DSS captures predominantly the dynamics of the slow and buried water molecules in deep, hydrophobic pockets and hence, reports a relaxation component which is markedly slower compared to bulk water.

Using computer simulations Makarov and Petit [83] found significant variation in residence times of water molecules at different sites of a protein. They detected as many as 294 hydration sites in myoglobin. The buried sites (e.g. cavities, grooves or concave surfaces) display a long residence time (>80 ps). In contrast, the exposed or convex sites are characterized by relatively short residence time (<10 ps). The residence times of a water molecule in a protein are in general, markedly longer than those in bulk water (0.34 ps and 4.1 ps). Bagchi and co-workers investigated solvation dynamics in a 36-residue globular protein, HP-36 [84, 85]. The secondary structure of this protein contains three short alpha-helices. The solvation dynamics of the polar amino acid residues in helix-2 ($\langle\tau\rangle = 11$ ps) is found to be twice as fast as that in the other two helices. Surprisingly, the water molecules around helix-2 exhibit much slower orientational dynamics than those around the other two helices. It is shown that the dynamics depends on the degree of exposure. An exposed water molecule displays fast solvation dynamics while a buried one exhibits slower dynamics.

Marchi and co-worker studied folding of a zwitterionic alanine octapeptide (A_8) in a reverse micelle (RM) by MD (molecular dynamics) simulation [86]. They showed that in the confined environment (RM), the folded structure of a protein is much more stable than the unfolded structure [86]. For a small RM, a stable helical structure of the polypeptide is detected. With rise in water content (w_0) as the size of water pool increases, the polypeptide forms an extended structure [86]. In a MD simulation, Zhong and co-workers detected multiple time scales of solvent relaxation in a peptide from femtosecond to tens of picoseconds [87].

Using terahertz spectroscopy and simulation, Heugen *et al*. showed that water molecules near a bio-molecule (lactose) are markedly slow [92]. They found that the hydration layer (up to which water dynamics is slow) around the carbohydrate extends up to 5.13 Å from the surface and contains 123 water molecules.

3.5. *Solvation dynamics in DNA*

Most recently, many groups have studied time dependent fluorescence Stokes shift in DNA [93–95]. Zewail and co-workers studied solvation dynamics in DNA using 2-aminopurine as an intrinsic probe and a minor groove binding non-covalent probe, pentamidine [93]. They detected a bi-exponential decay with an ultrafast sub-picosecond component due to bulk water and a relatively long (~10 ps) component. Berg and co-workers studied a series of oligo-nucleotides in which a native base pair is replaced by a dye molecule (C480) [94]. They found that when the probe (C480) is in the centre of the helix, the time scale of relaxation is broadly distributed over six decades of time scale from 40 fs to 40 ns and obeys a power law, $(1+\tau/\tau_0)^{-\alpha}$. The very long (~40 ns) component is assigned to the reorganization dynamics of DNA. Since the interior of the double helix is devoid of water, the observed Stokes shift seems to originate from the electric field of DNA on the probe. When the probe (C480) is attached at the end of the helix an additional very fast component of 5 ps is detected. The 5 ps component and the increased mobility ('fraying') at the end of the helix is ascribed to increased exposure of the probe to bulk water and lower counter-ion concentration [95].

Bagchi, Hynes and co-workers carried out a long (15 ns) simulation to explain the multiple time scale of relaxation times in DNA [96, 97]. Note, inside a DNA there is no water molecules and hence, solvation is dominated by electric field of the phosphate group and counter ions of DNA. In the major and minor groove however, there are a lot of water molecules. The solvation by the ions may give rise to the very long (~40 ns) component which is similar to formation time of ionic atmosphere. Most of the experiments so far [93–95] used relatively small oligo-nucleotides containing 17–20 base pairs. Such a small size precludes slow dynamics involving DNA chains. The simulations reveal a long (~250 ps) component of relaxation [96, 97].

3.6. *Solvation dynamics in a sol–gel glass and in ormosils*

In a sol–gel matrix (figure 1e) a silica surface surrounds a nanocage. As noted earlier water and many organic assemblies may be encaged in a sol–gel glass. The silica

surface is covered by Si–OH group. Eisenthal and co-workers showed that the OH group at a silica surface display two different pK_a – one loses a proton above pH = 4.5 and another at pH >12 [98]. Thus at a neutral pH (~7) there are a lot of negatively charged oxygen atoms. Sahu *et al*. investigated solvation dynamics in a sol–gel matrix doped with a cationic micelle (CTAB) [99]. There are two kinds of water molecules in this system. One is the relatively mobile water molecules at the core of the nanocage. The other group of water molecules are squeezed in between the silicate surface and cationic CTAB micelles and are largely immobilized. These two groups of water molecules give rise to a 120 ps and a 7200 ps component, respectively [99]. Sen *et al*. studied solvation dynamics of DCM inside a DPPC entrapped sol–gel matrix [100]. The main advantage a sol–gel matrix based on sodium silicate is that they may be prepared at a neutral pH without generation of alcohol. This ensures that the structure of the DPPC vesicle is intact inside the sol–gel matrix. Solvation dynamics inside sol–gel entrapped DPPC vesicle is retarded ~2.5 times compared to that in DPPC liposomes in bulk water [100]. The slow solvation dynamics is attributed to the restricted movement of the water molecules trapped in between the lipid vesicles and the sol–gel matrix.

4. Excited state proton transfer

Acidity of many molecules markedly increases in the excited state. For instance, pK_a of HPTS (8-hydroxypyrene-1,3,6-trisulfonate, HPTS) decreases from 7.4 in the ground state to 0.4 in the first excited state [101–104]. Thus an excited HPTS molecule rapidly transfers a proton to a water molecule even in a highly acidic media (e.g. pH ~ 1). The excited state proton transfer ESPT process in a photo-acid (ROH) may involve three steps – initial proton transfer (k_{PT}), recombination of the geminate ion pair (k_{rec}) and dissociation of the geminate pair into solvent separated ion pair (k_{diss}) (scheme 1).

The time evolution of the different species in scheme 1 is described by the following coupled differential equations [103]:

$$\frac{d}{dt}\begin{bmatrix} ROH \\ RO^- \cdots H^+ \\ RO^- \end{bmatrix} = \begin{bmatrix} -X & k_{rec} & 0 \\ k_{PT} & -Y & 0 \\ 0 & k_{diss} & -Z \end{bmatrix} \times \begin{bmatrix} ROH \\ RO^- \cdots H^+ \\ RO^- \end{bmatrix} \tag{5}$$

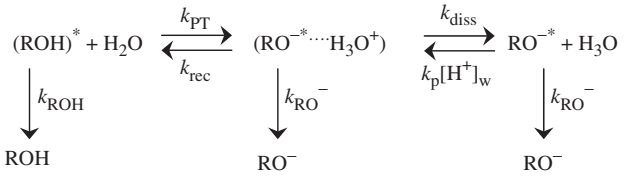

Scheme 1. Photophysical processes of an ESPT probe (ROH).

where,

$$X = k_{PT} + k_{ROH} \approx k_{PT}$$
$$Y = k_{rec} + k_{diss} + k_{RO^-}$$
$$Z = k_{RO^-}.$$

Very recently, Fayer and co-workers attempted to delineate the different steps involved in the ESPT process of HPTS in bulk water [104]. According to them, in bulk water HPTS at first undergoes solvation dynamics in ~1 ps. This is followed by a bi-exponential decay of 3 ps and 88 ps. The bi-exponential decay is analysed in terms of scheme 1 [104].

In an aqueous solution, HPTS may transfer a proton to an acetate to form acetic acid. This process may be studied by monitoring the rise of the carbonyl IR band at 1720 cm^{-1} arising from acetic acid. The rise of this band clearly monitors arrival of the proton to the acetate ion. Recently, several groups have used femtosecond transient absorption in the mid-IR region to study ESPT from HPTS to acetate [105–107]. For those HPTS molecules which are hydrogen bonded to the acetate in the ground state, the ESPT occurs in <150 fs (0.15 ps) [105–107]. For complexes where HPTS and acetate are separated by water molecules, the overall proton transfer time is 6 ps and is likely to occur through a Grotthuss-type proton transfer [105, 106]. Mohammed *et al*. showed that proton transfer from HPTS to monochloroacetate ($^-$OAc–Cl) in D_2O involve 'loose complexes' with D_2O bridges separating HPTS and $^-$OAc–Cl [107]. They proposed that proton transfer involves three steps. In the first step, the deuteron is transferred to the D_2O to form an intermediate ($HPTS^- \cdots D_3O^+ \cdots {}^-OAc–Cl$). This photo-acid dissociation process occurs within 150 fs. Then the deuteron is transferred to the acetate in 25 ps to form the 'loose' product complex ($HPTS^- \cdots D_2O \cdots DOAc–Cl$). Finally, the product complex dissociates in 50 ps in a diffusion controlled process.

ESPT in an organized assembly differs markedly from that in bulk water. Firstly, the local pH or pK_a of the acid may be very different from those in the bulk because of the differences in the polarity and the presence of counter-ion and consequent, electrostatic interactions. The absorption spectra of the protonated (ROH) and de-protonated (RO^-) form of HPTS are very different. Thus HPTS may utilize as a pH indicator. Using the absorption spectra of HPTS, Roy *et al*. estimated pH at the surface of a cationic micelle (CTAB) [108]. They found that at a bulk pH 7, the pH at the surface of CTAB micelle is ~9.5. The pH shift by 2.5 indicates that the proton concentration at the surface of the cationic micelle is smaller by more than two orders of magnitude compared to that in bulk water.

Confinement of an acid slows down the initial dissociation because of ultraslow solvent response and accelerates the recombination of the geminate ion-pair because of close proximity. Mondal *et al*. investigated ESPT of HPTS in γ-cyclodextrin (γ-CD) cavity using picosecond and femtosecond fluorescence spectroscopy [109]. They showed that the recombination of the geminate ion pair is accelerated but the initial proton transfer step and the dissociation of the geminate ion pair slow down inside a γ-CD cavity. Several groups used MD simulations to understand ESPT in a nanocavity [110, 111]. MD simulation and electrostatic potential calculations suggest that at the

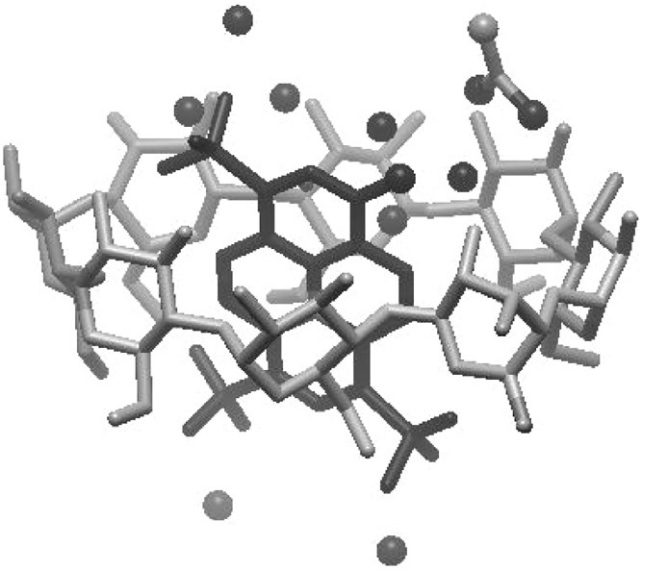

Figure 7. Optimized structure of the γ-CD:HPTS:acetate along with water molecules. Black spheres represent the oxygen atom of HPTS, acetate ion, and water. (Reprinted with permission from [114]. Copyright © 2006 American Chemical Society.)

rim of the cyclodextrin because of its interaction with the CD cavity the proton donor/acceptor property of water molecules is seriously impaired [110]. Sahu *et al.* showed that deprotonation, recombination and dissociation of the geminate ion pair in the lysozyme-CTAB aggregate are faster than that in a CTAB micelle [112].

At the surface of the micelle, emission of HPTS is quenched by acetate ion with a bimolecular quenching constant, $3.5 \times 107\,M^{-1}\,sec^{-1}$ [108]. This is markedly slower than the ESPT in a solvent separated HPTS–water–acetate complex in bulk water. It is interesting to note that even at very high local concentration of acetate ($\sim$7.75 M) in the Stern layer, the rate of proton transfer from HPTS to acetate occurs in 1300–2050 ps time scale [108]. This is an order of magnitude slower than the time constant (6 ps) of ESPT in solvent separated HPTS–water–acetate system in bulk water [113]. The slow ESPT at the micellar surface compared to bulk water may be ascribed to the rigidity of water hydrogen bond net work in the Stern layer of the micelle.

Most recently, Mondal *et al.* [114] reported that ESPT from HPTS to acetate inside a γ-cyclodextrin (γ-CD) and a hydroxypropyl γ-nanocavity (Hp-γ-CD) occurs in $\sim$90 ps which is much slower than that in bulk water. The structure of the supramolecule consisting of (γ-CD, HPTS, acetate and a few water molecules is optimized using MM2 and the structure is shown in figure 7 [114]. As shown in figure 7, the acetate group does not make a direct hydrogen bond to the OH group of HPTS (distance $\sim$4 Å). Instead, the acetate group remains hydrogen bonded to the two OH groups of the γ-CD. The OH group of HPTS is also hydrogen bonded to an OH group of γ-CD. Inside the γ-CD cavity, the acetate is separated from the OH group of HPTS by two water molecules as bridges [114]. In this case, proton transfer from HPTS to acetate is not direct and is

mediated by water bridges and thus resembles the Grotthuss mechanism. Obviously, in the cavity ESPT from HPTS to acetate requires rearrangement of the hydrogen bond network and the cyclodextrin cavity. In 40 mM γ-CD, the rate of initial proton transfer process (k_{PT}) increases ~3 times from $4.0 \pm 0.4 \times 10^{-3}\,ps^{-1}$ at 0 M acetate to $11 \pm 2.0 \times 10^{-3}\,ps^{-1}$ at 2 M acetate. In contrast, in the case of Hp-γ-CD the initial proton transfer rate (k_{PT}) remains almost unaffected on addition of acetate. It seems that the hydroxypropyl group of Hp-γ-CD shields the encapsulated HPTS molecule from the acetate. Hence, it is more difficult for the acetate to access HPTS in Hp-γ-CD than in unsubstituted γ-CD. As a result, ESPT in Hp-γ-CD is much slower [114].

5. Photoinduced electron transfer

Photoinduced electron transfer (PET) plays a fundamental role in many chemical and biological processes [115]. Because of the confinement of a donor and an acceptor at a close distance and hence, PET in an organized assembly is expected to be faster than that in bulk solvent. The classic Marcus electron transfer theory assumes equilibration of solvent at each point along the reaction coordinate which is defined as solvation [115, 116]. This theory predicts a bell shaped dependence of rate of electron transfer (ET) on the free energy change. Yoshihara and co-workers first reported that in liquid DMA (dimethyl aniline) PET exhibits a component faster than the solvation time [117–119]. Interestingly, even for ultrafast PET, they observed a bell shaped dependence of PET rate on free energy change (ΔG) and thus detected the so called Marcus inverted region. Bagchi and co-workers developed a non-Markovian model and correlated the highly non-exponential ET process with the highly non-exponential solvation dynamics [116]. They showed that solvent relaxation is important to bring about the ultrafast electron transfer observed by Yoshihara and co-workers.

Several authors suggested that ET is strongly influenced by factors other than solvent relaxation time [120–123]. Ovnichinnikova [121]. Zusman [122] and later Sumi and Marcus [123] considered the role of vibrational modes in an irreversible stochastic model of ET. This led to the so called 2D-ET model [123]. This model involves a solvent polarization coordinate (X) and a low frequency classical vibrational coordinate (Q). According to this model, the relaxation along Q is much faster than that along X and the effect of Q is included using a position dependent rate constant, $k(X)$.

A micelle or cyclodextrin cavity is an interesting system to study the effect of slow solvation dynamics and proximity of the donor and acceptor on PET. A detailed calculation of solvent reorganization energy and free energy change suggests that the rate of PET in a micelle increases with the increase of the chain length of the surfactant [124, 125]. Using a femtosecond up-conversion set up, Ghosh *et al*. studied ultrafast components PET (<10 ps) of in a micelle [126] and in a hydroxyl propyl γ-cyclodextrin cavity [127]. For three coumarin dyes (C481, C152 and C151), PET is found to be faster than solvation dynamics and hence, no rise is observed at the red end in the presence of the quencher. However, for C480 the fluorescence transient continues to exhibit a rise even at the highest concentration of the donor (DMA). This suggests that a part of solvation dynamics is slower than rate of PET in C480. In both the cases, a bell shaped

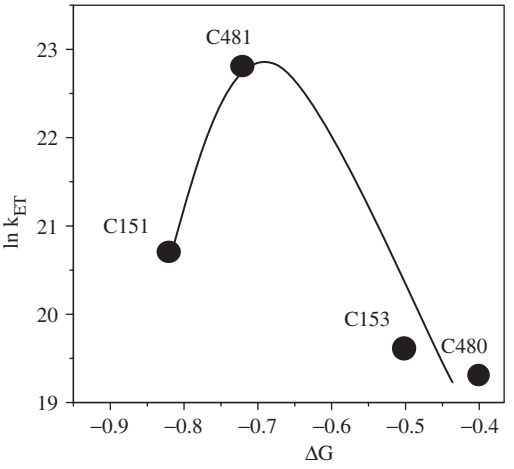

Figure 8. The ln(K_{ET}) vs. ΔG plot for coumarin-DMA system in 50 mM hpCD solution. (Reprinted with permission from [127]. Copyright © 2006 American Chemical Society.)

dependence of ultrafast PET on the free energy change (figure 8) is observed which is similar to Marcus inversion†.

PET across an interface plays an important role in biological systems. As a model, Eisenthal and co-workers studied ultrafast PET at DMA/water interface using femtosecond pump–probe surface sum frequency generation [128]. For this, they monitored the transient absorption of the product $DMA^{+\cdot}$ radical. They were able to determine the time constants of both forward and back electron transfer at the water surface.

6. Fluorescence resonance energy transfer

Fluorescence resonance energy transfer (FRET) inside an organized assembly is expected to be much faster than that in bulk water because of proximity of the donor and the acceptor. At a very short D–A distance, the electron clouds of donor and acceptor may overlap and basic assumptions of Forster theory (product wave functions and point-dipole approximation) may not be valid [7, 129, 130].

A micelle containing a donor and an acceptor is a simple system to study ultrafast FRET at a short distance. Usually, FRET is measured from the shortening of the fluorescence life time of the donor. For the donors with an acceptor in the immediate vicinity in the same micelle, the emission is strongly quenched and the lifetime becomes very short. The ultrafast component of the decay of these set of donors is missed in a picosecond set up [131].

The time constants of ultrafast FRET may be correctly determined if one studies the rise time of the acceptor emission (figure 9) using a femtosecond set up. Sahu *et al.* detected two ultrafast components (0.7 and 13 ps) of FRET are detected in a small SDS

†We prefer to describe this as similar but not the same as Marcus inversion because in this case the solvent is not at equilibrium (as assumed in Marcus theory).

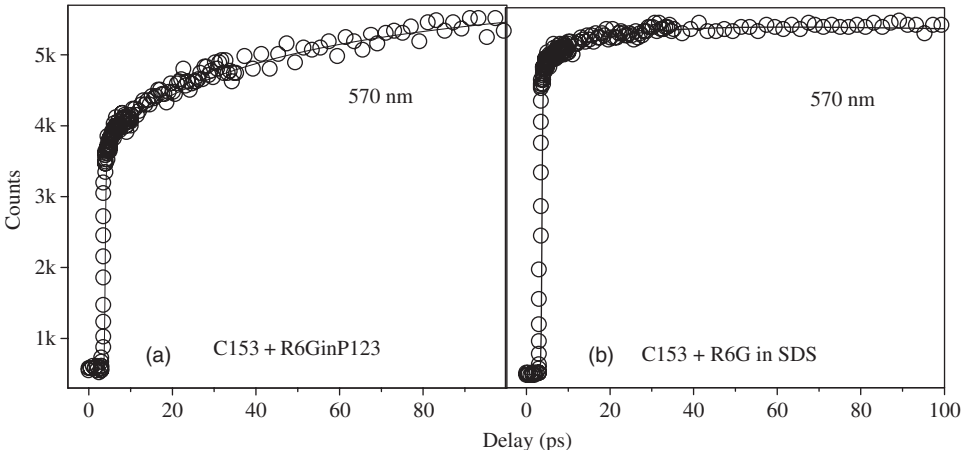

Figure 9. Femtosecond transients ($\lambda_{ex} = 405$ nm) of R6G (acceptor, $\lambda_{em} = 570$ nm) in the presence of C153 (donor) in (a) 1.74 mM P123 and (b) 55 mM SDS. (Reprinted with permission from [132]. Copyright © 2006 American Institute of Physics.)

(core radius ~20 Å) micelle from the rise time of the acceptor [132]. These two components correspond to Forster distances (R_{DA}) – 12 and 19 Å, respectively. In the big P123 micelle (core radius ~50 Å) in addition to the ultrafast components (1.2 and 24 ps corresponding to 12 Å and 20 Å), a long component of 1000 ps is observed. The long component (1000 ps) corresponds to a $R_{DA} = 44$ Å. The R_{DA} calculated from the ultrafast component is roughly equal to the donor–acceptor distance for direct contact and the R_{DA} calculated from the long component agrees well with micellar radius.

Mondal *et al*. studied the λ_{ex} dependence of FRET in AOT reverse micelle using C480 as donor and fluorescein 548 (F548) as acceptor [133]. The anionic acceptor resides inside the water pool while the donor (C480) is distributed over three locations – bulk heptane, AOT interface and the core of the water pool. They observed that inside AOT microemulsion FRET involves three time scales – 3 ps, 200 ps and 2700 ps. The 3 ps component is assigned to FRET in the water pool of the reverse micelle at a donor–acceptor distance 16 Å. The 200 ps component corresponds to a donor–acceptor distance 30 Å and is ascribed to the negatively charged acceptor inside the water pool and the neutral donor inside the alkyl chains of AOT. The very long 2700 ps component arises from diffusion of the donor from bulk heptane to the reverse micelle. At $\lambda_{ex} = 375$ nm, C480 molecules in the bulk heptane are preferentially excited. At $\lambda_{ex} = 405$ nm, C480 inside the reverse micelle are excited. As a result, with increase in the excitation wavelength from 375 nm to 405 nm the relative contribution of the FRET due to C480 in the AOT reverse micelle (3 ps and 200 ps components) increases [133].

7. Fluorescence anisotropy decay

Fluorescence anisotropy decay refers to the decay of optical anisotropy created in a isotropic ensemble of molecules by excitation by a polarized light. The time dependent

fluorescent anisotropy is given by

$$r(t) = \frac{I_{\parallel}(t) - GI_{\perp}(t)}{I_{\parallel}(t) + 2GI_{\perp}(t)} \tag{6}$$

where $I_{\parallel}(t)$ and $I\perp(t)$ are time dependent emission intensities polarized, respectively parallel and perpendicular to the polarization of the exciting light pulse and G is a correction factor arising from the anisotropic response of the instrument. The anisotropy decay arises from the rotation of the excited molecules and is thus monitors rotational dynamics. The hydrodynamic radius (r_h) of the complexes may be estimated from the time constant (τ_R) of fluorescence anisotropy decay using the equation

$$\tau_R = \frac{4\pi\eta r_h^3}{3kT}. \tag{7}$$

Thus the rotational decay gives an estimate of the effective volume (V) of the rotating molecular species and hence, gives structural information. Note, X-ray diffraction is inapplicable in the case of a liquid. Thus anisotropy decay is a valuable technique to get structural information in a liquid.

We will illustrate with the anisotropy decay of C153 inside di- and tri-methyl β-CD [40]. Anisotropy decay of this supramolecule displays a bi-exponential decay with components 1000–1150 ps and 2500–2700 ps. The two components are ascribed respectively to the 1:1 and 1:2 complex of C153 with cyclodextrin. The hydrodynamic radius of the 1:1 and 1:2 complexes are 8.5 ± 0.5 and 11.5 ± 0.5 Å, respectively. Since the height of dimethyl β-CD is 10.9 Å, it appears that ~5 Å the probe is projected out of the cavity in case of the 1:1 complex. The hydrodynamic diameter ($2r_h$) of 1:2 complex is roughly equal to the sum of height of two CD cavities. Douhal and co-workers studied encapsulation of several drug molecules in cyclodextrins [134–136]. They reported that the fluorescence lifetime of a drug, milrinone (MIR) increases from 65 ps in bulk water to 240–350 ps on confinement in cyclodextrins (α-, β-, γ-CD and dimethyl-β-CD). From anisotropy decay and PM3 calculations, they concluded that the drug is not fully encaged inside the cavity.

Most recently, Roy *et al.* observed an extremely slow anisotropy decay (time constant > 20 ns) for the C153-γ-cyclodextrin guest–host complex (figure 10) [43]. They attributed the ultraslow time constant of anisotropy to the formation of a long nanotube aggregate containing a large number (>50) cyclodextrins joined together non-covalently through the guest molecules (figure 10).

8. Conclusion

In this article, we have given a broad overview of the unusual dynamics in many organized assemblies. For this purpose, we used mainly the ultrafast fluorescence spectroscopy for its superior time and special resolution. The results outlined in this article conclusively demonstrate that chemistry in a confined system is substantially

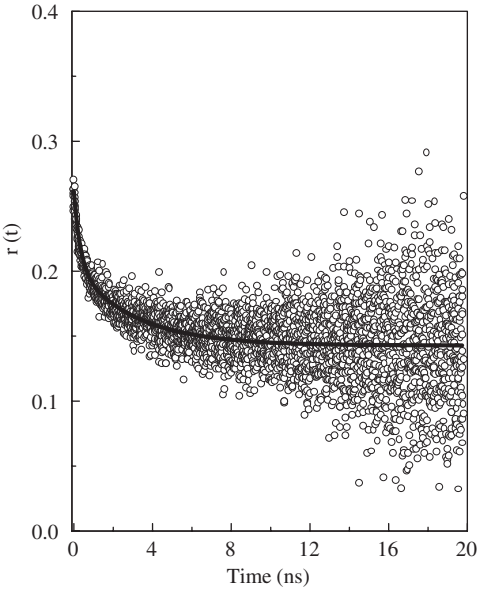

Figure 10. Fluorescence anisotropy decay of C153 ($\lambda_{ex} = 405$ nm and $\lambda_{em} = 490$ nm in) 40 mM γ-CD at 278 K. (Reprinted with permission from [43]. Copyright © 2005 American Chemical Society.)

different from that in a liquid. Confinement, organization and local interactions dramatically modify the dynamics of ultrafast chemical processes in a nanocavity. The results outlined in this review have widespread implications in biology – in particular in drug delivery, molecular recognition and formation of nanostructures. The recent application of ultrafast spectroscopy in biological system may ultimately explain the complex chemistry of these systems in atomistic details. The final goal is what Feynman [137] dreamt about 40 years ago, 'everything that living things do can be understood in terms of jigglings and wigglings of atoms'.

Acknowledgements

Thanks are due to the Department of Science and Technology, India (Project Number: IR/I1/CF-01/2002) and the Council of Scientific and Industrial Research (CSIR) for generous research grants. SG, UM, AA and SD thank CSIR for awarding fellowships.

References

[1] B. Bagchi, Chem. Rev. **105,** 3197 (2005).
[2] S. K. Pal and A. H. Zewail, Chem. Rev. **104,** 2099 (2004).
[3] R. A. Farrer and J. T. Fourkas, Acc. Chem. Res. **36,** 605 (2003).
[4] K. Bhattacharyya, Acc. Chem. Res. **36,** 95 (2003).
[5] R. Richert, J. Chem. Phys. **113,** 8404 (2000).
[6] N. Nandi, K. Bhattacharyya, and B. Bagchi, Chem. Rev. **100,** 2013 (2000).
[7] J. R. Lakowicz, *Principles of Fluorescence Spectroscopy*, 3rd ed. (Kluwer, Dordrecht, 2006).

[8] S. Berr, R. R. M. Jones, and J. S. Johnson Jr, J. Phys. Chem. **96,** 5611 (1992).
[9] K. Streletzky and G. D. J. Phillies, Langmuir **11,** 42 (1995).
[10] W. Brown, R. Rymden, J. van Stam, M. Almgren, and G. Svensk, J. Phys. Chem. **93,** 2512 (1989).
[11] W. Saenger, in *Inclusion Compounds*, edited by J. L. Atwood, J. E. D. Davis, and D. D. MacNicol (Academic Press, New York, 1984), Vol. 2, p. 231.
[12] K. Uekama, F. Hirayama, and T. Irie, Chem. Rev. **98,** 2045 (1998).
[13] M. Khajehpour, T. Troxler, V. Nanda, and J. M. Vanderkooi, Proteins **55,** 275 (2004).
[14] P. Alexandridis, U. Olsson, and B. Lindman, Langmuir **14,** 2627 (1998).
[15] R. Ganguly, V. K. Aswal, P. A. Hassan, I. K. Gopalakrishnan, and J. V. Yakhmi, J. Phys. Chem. B **109,** 5653 (2005).
[16] C. D. Grant, K. E. Steege, M. R. Bunagan, and E. W. Castner Jr, J. Phys. Chem. B **109,** 22273 (2005).
[17] C. D. Grant, M. R. DeRitter, K. E. Steege, T. A. Fadeeva, and E. W. Castner Jr, Langmuir **21,** 1745 (2005).
[18] A. Maitra, J. Phys. Chem. **88,** 5122 (1984).
[19] N. M. Correa and N. Levinger, J. Phys. Chem. B **110,** 13050 (2006).
[20] B. Baruah, J. M. Roden, M. Sedgwick, N. M. Correa, D. C. Crans, and N. E. Levinger, J. Am. Chem. Soc. **128,** 12758 (2006).
[21] I. R. Piletic, D. E. Moilanen, D. B. Spry, N. E. Levinger, and M. D. Fayer, J. Phys. Chem. B **110,** 4985 (2006).
[22] G. M. Sando, K. Dahl, and J. C. Owrutsky, J. Phys. Chem. B **109,** 4084 (2005).
[23] R. Nörenberg, J. Klingler, and D. Horn, Angew. Chem. Int. Ed. **38,** 1626 (1999).
[24] C. J. Binker and G. W. Scherer, *Sol–Gel Science* (Academic Press, San Diego, 1990),.
[25] J. D. Jordan, R. A. Dunbar, and F. V. Bright, Anal. Chem. **67,** 2436 (1995).
[26] T. Besanger, Y. Zhang, and J. D. Brennan, J. Phys. Chem. B **106,** 10535 (2002).
[27] R. Jimenez, G. R. Fleming, P. V. Kumar, and M. Maroncelli, Nature **369,** 471 (1994).
[28] N. Nandi, S. Roy, and B. Bagchi, J. Chem. Phys. **102,** 1390 (1995).
[29] C. J. Fecko, J. D. Eaves, J. J. Loparo, A. Tokmakoff, and P. L. Geissler, Science **301,** 1698 (2003).
[30] G. Otting, E. Liepinsh, and K. Wuthrich, Science **254,** 974 (1991).
[31] N. Nandi and B. Bagchi, J. Phys. Chem. B **101,** 10954 (1997); J. Phys. Chem. A **102,** 8217 (1998).
[32] M. Levitt and R. Sharon, Proc. Natl. Acad. Sci. USA **85,** 7557 (1988).
[33] S. Pal, S. Balasubramanian, and B. Bagchi, J. Phys. Chem. B **107,** 5194 (2003).
[34] A. A. Golosov and M. Karplus, J. Phys. Chem. B **111,** 1482 (2007).
[35] I. Benjamin, Chem. Rev. **106,** 1212 (2006).
[36] D. Michael and I. Benjamin, J. Chem. Phys. **114,** 2817 (2001).
[37] G. Srinivas, K. L. Sebastian, and B. Bagchi, J. Chem. Phys. **116,** 7276 (2002).
[38] N. Nandi and B. Bagchi, J. Phys. Chem. **100,** 13914 (1996).
[39] S. Vajda, R. Jimenez, S. J. Rosenthal, V. Fidler, G. R. Fleming, and E. W. Castner Jr, J. Chem. Soc. Faraday Trans. **91,** 867 (1995).
[40] P. Sen, D. Roy, S. K. Mondal, K. Sahu, S. Ghosh, and K. Bhattacharyya, J. Phys. Chem. A **109,** 9716 (2005).
[41] S. Sen, D. Sukul, P. Dutta, and K. Bhattacharyya, J. Phys. Chem. A **105,** 10635 (2001).
[42] P. Sen, S. Mukherjee, A. Halder, and K. Bhattacharyya, Chem. Phys. Lett. **385,** 357 (2004).
[43] D. Roy, S. K. Mondal, K. Sahu, S. Ghosh, P. Sen, and K. Bhattacharyya, J. Phys. Chem. A **109,** 7359 (2005).
[44] K. Sahu, S. K. Mondal, S. Ghosh, D. Roy, P. Sen, and K. Bhattacharyya, J. Chem. Phys. **124,** 124909 (2006).
[45] A. P. Demchenko, Biophys. Chem. **15,** 101 (1982).
[46] J. R. Lakowicz, Biochemistry **23,** 3013 (1984).
[47] D. A. Kelkar and A. Chattopadhyay, J. Phys. Chem. B **108,** 12151 (2004).
[48] T. Satoh, H. Okuno, K. Tominaga, and K. Bhattacharyya, Chem. Lett. **33,** 1090 (2004).
[49] P. Sen, T. Satoh, K. Bhattacharyya, and K. Tominaga, Chem. Phys. Lett. **411,** 339 (2005).
[50] P. Sen, S. Ghosh, S. K. Mondal, K. Sahu, D. Roy, K. Bhattacharyya, and K. Tominaga, Chem. Asian. J. **1,** 188 (2006).
[51] P. Sen, S. Ghosh, K. Sahu, S. K. Mondal, D. Roy, and K. Bhattacharyya, J. Chem. Phys. **124,** 204905 (2006).
[52] S. Ghosh, A. Adhikari, U. Mandal, S. Dey, and K. Bhattacharyya, J. Phys. Chem. C (2007, web published date 02/22/2007, DOI: 1021/jp067042f).
[53] P. Mukherjee, J. A. Crank, M. Halder, D. W. Armstrong, and J. W. Petrich, J. Phys. Chem. A **110,** 10725 (2006).
[54] D. Seth, A. Chakraborty, P. Setua, and N. Sarkar, Langmuir **22,** 7768 (2006).
[55] S. Pal, B. Bagchi, and S. Balasubramanian, J. Phys. Chem. B **109,** 12879 (2005).
[56] S. Senapati and M. L. Berkowitz, J. Chem. Phys. **118,** 1937 (2003).

[57] J. Faeder and B. M Ladanyi, J. Phys. Chem. B **109,** 6732 (2005).
[58] M. R. Harpham, B. M. Ladanyi, and N. E. Levinger, J. Phys. Chem. B **109,** 16891 (2005).
[59] C. N. Ramachandran and N. Sathyamurthy, Chem. Phys. Lett. **410,** 348 (2005).
[60] S. Senapati and A. Chandra, J. Phys. Chem. B **105,** 5106 (2001).
[61] W. H. Thompson, J. Chem. Phys. **120,** 8125 (2004).
[62] J. A. Gomez and W. H. Thompson, J. Phys. Chem. B **108,** 20144 (2004).
[63] T. S. Gulmen and W. H. Thompson, Langmuir **22,** 10919 (2006).
[64] P. Hirunsit and P. B. Balbuena, J. Phys. Chem. C **111,** 1709 (2007).
[65] P. Dutta, P. Sen, S. Mukherjee, A. Halder, and K. Bhattacharyya, J. Phys. Chem. B **107,** 10815 (2003).
[66] L. P. McMahon, H. T. Yu, M. A. Vela, G. A. Morales, L. Shui, F. R. Fronczek, M. L. McLaughlin, and M. D. Barkley, J. Phys. Chem. B **101,** 3269 (1997).
[67] J. T. Vivian and P. R. Callis, Biophys. J. **80,** 2093 (2001).
[68] C. Dedonder-Lardeux, C. Jouvet, S. Perun, and A. L. Soblewski, Phys. Chem. Chem. Phys. **5,** 5118 (2003).
[69] X. J. Jordanides, M. J. Lang, X. Song, and G. R. Fleming, J. Phys. Chem. B **103,** 7995 (1999).
[70] S. K. Pal, D. Mandal, D. Sukul, S. Sen, and K. Bhattacharyya, J. Phys. Chem. B **105,** 1438 (2001).
[71] P. Dutta, P. Sen, S. Mukherjee, and K. Bhattacharyya, Chem. Phys. Lett. **382,** 426 (2003).
[72] P. Dutta, P. Sen, A. Halder, S. Mukherjee, S. Sen, and K. Bhattacharyya, Chem. Phys. Lett. **377,** 229 (2003).
[73] B. C. Cohen, T. B. McAnaney, E. S. Park, Y. N. Jan, S. G. Boxer, and L. Y. Jen, Science **296,** 1700 (2002).
[74] D. Mandal, S. Sen, D. Sukul, K. Bhattacharyya, A. K. Mandal, R. Banerjee, and S. Roy, J. Phys. Chem. B **106,** 10741 (2002).
[75] S. Guha, K. Sahu, D. Roy, S. K. Mondal, S. Roy, and K. Bhattacharyya, Biochemistry **44,** 8940 (2005).
[76] V. P. Denisov, B.-H. Jonsson, and B. Halle, Nature Srtuct. Biol. **6,** 253 (1999).
[77] P. Sen, S. Mukherjee, P. Dutta, A. Halder, D. Mandal, R. Banerjee, S. Roy, and K. Bhattacharyya, J. Phys. Chem. B **107,** 14563 (2003).
[78] K. Chattopadhyay and S. Mazumdar, Biochemistry **42,** 14606 (2003).
[79] K. Sahu, S. K. Mondal, S. Ghosh, D. Roy, P. Sen, and K. Bhattacharyya, J. Phys. Chem. B **110,** 1056 (2006).
[80] S. Samaddar, A. K. Mandal, S. K. Mondal, K. Sahu, K. Bhattacharyya, and S. Roy, J. Phys. Chem. B **110,** 21210 (2006).
[81] P. Sen, D. Roy, K. Sahu, S. K. Mondal, and K. Bhattacharyya, Chem. Phys. Lett. **395,** 58 (2004).
[82] M. Maroncelli and G. R. Fleming, J. Chem. Phys. **88,** 5044 (1988).
[83] V. Makarov and B. M. Petit, Acc. Chem. Res. **35,** 376 (2002).
[84] S. Bandyopadhyay, S. Chakraborty, and B. Bagchi, J. Am. Chem. Soc. **127,** 16660 (2005).
[85] S. Bandyopadhyay, S. Chakraborty, S. Balasubramanian, and B. Bagchi, J. Am. Chem. Soc. **127,** 4071 (2005).
[86] S. Abel, M. Waks, W. Urbach, and M. Marchi, J. Am. Chem. Soc. **128,** 382 (2006).
[87] A. A. Hassanali, T. P. Li, D. P. Zhong, and S. J. Singer, J. Phys. Chem. B **110,** 10497 (2006).
[88] L. Nilsson and B. Halle, Proc. Natl. Acad. Sci. U.S.A. **102,** 13867 (2005).
[89] C. Caronna, F. Natali, and A. Cupane, Biophys. Chem. **116,** 219 (2005).
[90] D. Russo, R. K. Murarka, J. R. D. Copley, and T. Head-Gordon, J. Phys. Chem. B **109,** 12966 (2005).
[91] K. Modig, E. Liepinsh, G. Otting, and B. Halle, J. Am. Chem. Soc. **126,** 102 (2004).
[92] U. Heugen, G. Schwaab, E. Brundermann, M. Heyden, X. Yu, D. M. Leitner, and M. Havenith, Proc. Natl. Acad. Sci. U.S.A. **103,** 12301 (2006).
[93] S. K. Pal, L. Zhao, T. Xia, and A. H. Zewail, Proc. Natl. Acad. Sci. U.S.A. **100,** 13746 (2003).
[94] D. Andreatta, J. L. P. Lustres, S. A. Kovalenko, N. P. Ernsting, C. J. Murphy, R. S. Coleman, and M. A. Berg, J. Am. Chem. Soc. **127,** 7270 (2005).
[95] D. Andreatta, S. Sen, J. L. P. Lustres, S. A. Kovalenko, N. P. Ernsting, C. J. Murphy, R. S. Coleman, and M. A. Berg, J. Am. Chem. Soc. **128,** 6885 (2006).
[96] B. Jana, S. Pal, P. K. Maiti, S. T. Lin, J. T. Hynes, and B. Bagchi, J. Phys. Chem. B **110,** 19611 (2006).
[97] S. Pal, P. K. Maiti, B. Bagchi, and J. T. Hynes, J. Phys. Chem. B **110,** 26396 (2006).
[98] S. Ong, X. Zhao, and K. B. Eisenthal, Chem. Phys. Lett. **191,** 327 (1992).
[99] K. Sahu, D. Roy, S. K. Mondal, A. Halder, and K. Bhattacharyya, J. Phys. Chem. B **108,** 11971 (2004).
[100] P. Sen, S. Mukherjee, A. Patra, and K. Bhattacharyya, J. Phys. Chem. B **109,** 3319 (2005).
[101] K. K. Smith, K. J. Kaufmann, D. Huppert, and M. Gutman, Chem. Phys. Lett. **64,** 522 (1979).
[102] N. Agmon, J. Phys. Chem. A **109,** 13 (2005).
[103] L. Giestas, C. Yihwa, J. C. Lima, C. Vautier-Giongo, A. Lopes, A. L. Macanita, and F. H. Quina, J. Phys. Chem. A **107,** 3263 (2003).
[104] D. B. Spry, A. Goun, and M. D. Fayer, J. Phys. Chem. A **111,** 230 (2007).
[105] M. Rini, B.-Z. Magnes, E. Pines, and E. T. J. Nibbering, Science **301,** 349 (2003).

[106] M. Rini, D. Pines, B.-Z. Magnes, E. Pines, and E. T. J. Nibbering, J. Chem. Phys. **121,** 9593 (2004).
[107] O. Mohammed, D. Pines, J. Dryer, E. Pines, and E. T. J. Nibbering, Science **310,** 83 (2005).
[108] D. Roy, R. Karmakar, S. K. Mondal, K. Sahu, and K. Bhattacharyya, Chem. Phys. Lett. **399,** 147 (2004).
[109] S. K. Mondal, K. Sahu, P. Sen, D. Roy, S. Ghosh, and K. Bhattacharyya, Chem. Phys. Lett. **412,** 228 (2005).
[110] R. Gepshtein, P. Leiderman, D. Huppert, E. Project, E. Nachliel, and M. Gutman, J. Phys. Chem. B **110,** 26354 (2006).
[111] W. H. Thompson, J. Phys. Chem. B **109,** 18201 (2005).
[112] K. Sahu, D. Roy, S. K. Mondal, R. Karmakar, and K. Bhattacharyya, Chem. Phys. Lett. **404,** 341 (2005).
[113] L. T. Genosar, B. Cohen, and D. Huppert, J. Phys. Chem. A **104,** 6689 (2000).
[114] S. K. Mondal, K. Sahu, S. Ghosh, P. Sen, and K. Bhattacharyya, J. Phys. Chem. A **110,** 13646 (2006).
[115] R. A. Marcus, Adv. Chem. Phys. **106,** 1 (1999).
[116] B. Bagchi and N. Gayathri, Adv. Chem. Phys. **107,** 1 (1999).
[117] K. Yoshihara, Adv. Chem. Phys. **107,** 371 (1999).
[118] H. Pal, Y. Nagasawa, K. Tominaga, and K. Yoshihara, J. Phys. Chem. **100,** 11964 (1996).
[119] H. Shirota, H. Pal, K. Tominaga, and K. Yoshihara, J. Phys. Chem. A **102,** 3089 (1998).
[120] P. F. Barbara and E. J. J. Olson, Adv. Chem. Phys. **107,** 647 (1999).
[121] M. Y. Ovnichinnikova, Theor. Exp. Chem. **17,** 507 (1982).
[122] L. D. Zusman, Chem. Phys. **80,** 29 (1983).
[123] H. Sumi and R. A. Marcus, J. Chem. Phys. **84,** 4894 (1986).
[124] H. L. Tavernier, A. V. Barzykin, M. Tachiya, and M. D. Fayer, J. Phys. Chem. B **102,** 6078 (1998).
[125] A.V. Barzykin, K. Seki, and M. Tachiya, J. Phys. Chem. B **103,** 9156 (1999).
[126] S. Ghosh, K. Sahu, S. K. Mondal, P. Sen, and K. Bhattacharyya, J. Chem. Phys. **125,** 054509 (2006).
[127] S. Ghosh, S. K. Mondal, K. Sahu, and K. Bhattacharyya, J. Phys. Chem. A **110,** 13139 (2006).
[128] E. A. McArthur and K. B. Eisenthal, J. Am. Chem. Soc. **128,** 1068 (2006).
[129] S. Bhowmick, S. Saini, V. B. Shenoy, and B. Bagchi, J. Chem. Phys. **125,** 181102 (2006).
[130] C. S. Yun, A. Javier, T. Jennings, M. Fisher, S. Hira, S. Peterson, B. Hopkins, N. O. Reich, and G. F. Strouse, J. Am. Chem. Soc. **127,** 3115 (2005).
[131] D. Seth, D. Chakrabarty, A. Chakraborty, and N. Sarkar, Chem. Phys. Lett. **401,** 546 (2005).
[132] K. Sahu, S. Ghosh, S. K. Mondal, B. C. Ghosh, P. Sen, D. Roy, and K. Bhattacharyya, J. Chem. Phys. **125,** 044714 (2006).
[133] S. K. Mondal, S. Ghosh, K. Sahu, U. Mandal, and K. Bhattacharyya, J. Chem. Phys. **125,** 224710 (2006).
[134] M. El-Kemary, J. A. Organero, L. Santos, and A. Douhal, J. Phys. Chem. B **110,** 14128 (2006).
[135] A. Douhal, M. Sanz, and L. Tormo, Proc. Nat. Acad. Sci. USA **102,** 18807 (2005).
[136] L. Tormo, J. A. Organero, and A. Douhal, J. Phys. Chem. B **109,** 17848 (2005).
[137] R. P. Feynman, R. B. Leighton, and M. Sands, *The Feynman Lectures in Physics* (Addison Wesley, Reading, 1963), Vol. 1, p. 3.